NEMS-Based Infrared Metamaterial via Tuning Nanocantilevers Within Complementary Split Ring Resonators

Qiugu Wang, Depeng Mao, Peng Liu, Thomas Koschny, Costas M. Soukoulis, and Liang Dong

***Abstract*— Dynamic control of the electromagnetic properties of metamaterials requires wide modulation bandwidth. Tunable metamaterials with large tunability and fast speed are thus highly desirable. Due to the small dimensions, subwavelength meta-atoms or resonant elements that constitute a metamaterial in the mid-to-near-infrared (IR) wavelength range are often not easy to be tuned at a high rate of several tens of megahertz (MHz). Here, we report on a nanoelectromechanical systems (NEMS)-based tunable IR metamaterial realized by unique embedding of nanocantilevers into complementary split ring resonators (c-SRRs) suspended over individual wells. The optical field confined in the air gap of the c-SRR is strongly influenced by electrostatically induced mechanical deflection of the nanocantilever, thus modulating the reflection spectrum of the metamaterial. With the easy-to-implement tunable meta-atom design, the IR metamaterial with 800-nm-long cantilevers provides an ultrahigh mechanical modulation frequency of 32.26 MHz for optical signal modulation at a wavelength of 2.1 μm, and is rather easy to manufacture and operate. We envision a compact, efficient, and high-speed electrooptic modulation platform in the IR region using this NEMS tunable metamaterial technology. [2017-0012]**

***Index Terms*— Nanoelectromechanical systems (NEMS), metamaterial, nanocantilever, electro-optic modulation.**

I. Introduction

METAMATERIALS are artificially-engineered resonant structures that can be used to manipulate electromagnetic (EM) waves on subwavelength scales. They are promising for a variety of applications such as superlenses [1], [2], invisibility cloaks [3], [4], perfect absorbers [5], [6], and biochemical sensors [7]–[9]. The ever-increasing demand for active control of the EM properties of metamaterials has led to the development of tunable metamaterials [10], which are mainly realized by hybridizing meta-atoms or resonant elements with nonlinear materials such as phase-change media [11]–[13], liquid crystals [14]–[17] and semiconductors [18]–[20]. Alternatively, the microsystems technology has also enabled the realization of tunable metamaterials [21] by using thermally-actuated bimorph beams [22]–[25] and in-plane electrostatic comb drives [26]–[29]. This type of tunable metamaterials can be realized via the complementary-metal-oxide-semiconductor (CMOS) fabrication process to enable flexible control with integrated circuits [21]. Nevertheless, both the optical resonance wavelength and mechanical modulation frequency of these metamaterials are usually limited by the relatively large size of the tunable meta-atoms. For example, tunable near-infrared (IR) metamaterial-based absorbers [30], [31] have recently been developed via constructing diffractive nanohole gratings on a diaphragm with dimensions of hundred microns. They rely on sophisticated CMOS-compatible fabrication processes but only have modulation frequencies of the order of kilohertz. In order to improve the modulation frequency, multiple pairs of tens-of-microns-long metallic strings were previously arranged in parallel, and electrostatic [32] or optical [33] forces were applied to control nanoscale strip displacements at a rate of 1-2 MHz. Despite these efforts, tuning metamaterials at a rate of several tens of MHz in the near-IR and shorter-wavelength spectral region remains very challenging.

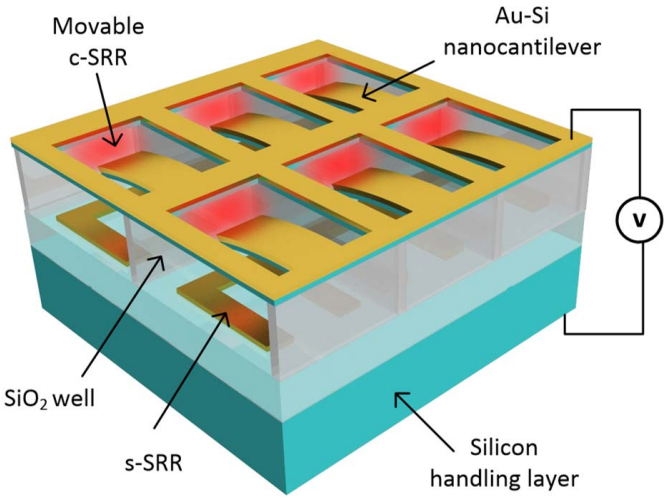

Fig. 1. Schematic of the NEMS-enabled tunable metamaterial operating in the near-to-mid-IR wavelength region.

Manuscript received January 16, 2017; revised July 8, 2017; accepted August 25, 2017. Date of publication September 12, 2017; date of current version November 29, 2017. This work was supported in part by the U.S. National Science Foundation under Grant ECCS-0954765 and Grant ECCS-1711839, and in part by the U.S. Department of Energy, Office of Basic Energy Science, Division of Materials Sciences and Engineering, under Contract DE-AC02-07CH11358. Subject Editor X. Zhang. *(Corresponding author: Liang Dong.)*

Q. Wang and L. Dong are with the Department of Electrical and Computer Engineering, Iowa State University, Ames, IA 50011 USA (e-mail: ldong@iastate.edu).

D. Mao was with the Department of Electrical and Computer Engineering, Iowa State University, Ames, IA 50011 USA. He is now with Microsoft Corporation, Redmond, WA 98052 USA.

P. Liu was with the Department of Electrical and Computer Engineering, Iowa State University, Ames, IA 50011 USA. He is now with Epic Systems Corporation, Verona, WI 53593 USA.

T. Koschny and C. M. Soukoulis are with the Ames Laboratory, United States Department of Energy, Iowa State University, Ames, IA 50011 USA, and also with the Department of Physics and Astronomy, Iowa State University, Ames, IA 50011 USA.

Color versions of one or more of the figures in this paper are available online at http://ieeexplore.ieee.org.

Digital Object Identifier 10.1109/JMEMS.2017.2746688

1057-7157 © 2017 IEEE. Personal use is permitted, but republication/redistribution requires IEEE permission.
See http://www.ieee.org/publications_standards/publications/rights/index.html for more information.

Authorized licensed use limited to: Iowa State University. Downloaded on June 04,2022 at 12:40:41 UTC from IEEE Xplore. Restrictions apply.

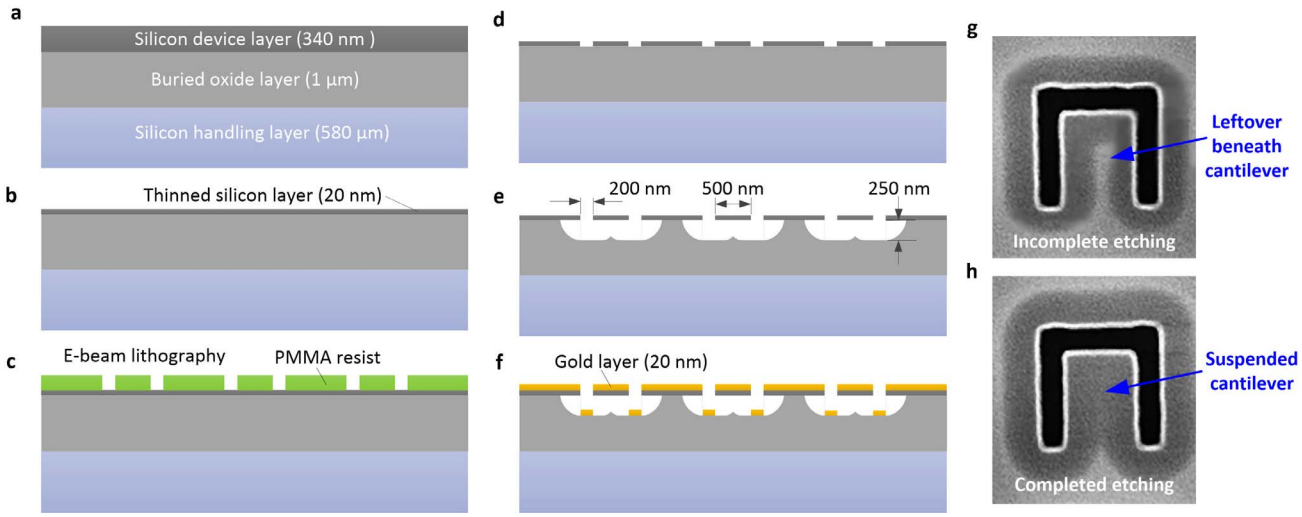

Fig. 2. (a)-(f) Schematic of the fabrication process for the tunable IR metamaterial. (g)-(h) SEM images showing an unreleased cantilever after BOE etching of buried oxide for 3.5 min (g), and a released cantilever after BOE etching of oxide for 5 min. The length of the cantilever in (g) and (h) is 800 nm.

Here, we report on a nanoelectromechanical systems (NEMS)-based reconfigurable metamaterial operating in the near-to-mid-IR region which affords ultrafast electro-optic modulation and is rather easy to fabricate and operate.

II. Device Structure and Principle

Fig. 1 schematically illustrates the working principle of the proposed metamaterial. The metamaterial is composed of an array of gold−silicon (Au−Si) bilayer complementary split ring resonators (c-SRRs) at the top and an array of Au solid SRRs (s-SRRs) at the bottom of SiO_2 wells. The c-SRR has an inverse shape to the s-SRR. An in-plane cantilever is embedded in the c-SRR and surrounded by a 200 nm-wide U-shaped air gap. The top c-SRRs are positioned 250 nm above the bottom of the SiO_2 well formed in a 1 μm-thick buried SiO_2 layer of a silicon-on-insulator (SOI) substrate. The cantilever is composed of 20 nm-thick Si and 20 nm-thick Au layers. One end of the cantilever is anchored while the other end is free to move. The cantilever is 800 nm long and 500 nm wide. The entire top Au layer serves as an electrode, while the Si handling layer of the SOI substrate is the other electrode of an electrostatic actuator. Depending on the polarization direction of incident light, different eigenmodes of the c-SRR or s-SRR structures of the metamaterial can be excited. When a voltage is applied between the top Au and bottom Si handling layers, the generated electrostatic force bends the embedded nanocantilever towards the bottom of the SiO_2 well (see Supplementary Movie 1). The electrostatically induced mechanical deflection of the nanocantilever changes the shape of the U-shaped air gap, thus allowing tuning of the characteristics of the optical resonant modes of the c-SRR or s-SRR. Profoundly, due to the compact design and small dimensions of the nanocantilever, the proposed metamaterial can be synchronously driven at modulation frequencies up to several tens of MHz to tune its reflection spectrum in the IR region, thus providing much faster electro-optic modulation than many other counterpart metamaterials [26]–[34]. Note that in this paper subwavelength meta-atoms refer to the c-SRR or s-SRR resonant units shown in Fig. 1.

III. Methods

A. Metamaterial Fabrication

The metamaterial design was implemented on a SOI wafer. Fig. 2 shows the schematic of the fabrication process for the metamaterial. The SOI wafer consisted of a 340-nm-thick device silicon layer, a 1-μm-thick buried oxide layer, and 580-μm-thick handling silicon wafer (Fig. 2a). First, the top silicon layer of the SOI substrate was thinned down to ~20 nm by thermal oxidation, with subsequent wet-etching of SiO_2using a buffered oxide etch (BOE) solution (Fig. 2b). Subsequently, the thinned silicon layer was doped with phosphorous ions (5×10^{19} cm^{-3}) to increase electrical conductivity for serving as a top electrode. U-shaped air gaps were then patterned in the thinned silicon layer by means of e-beam lithography (Fig. 2c) and subsequent reactive-ion etching of silicon (Fig. 2d); thus, the patterns of the nanocantilever array were formed. Next, the wafer was immersed into the BOE solution for 5 min to totally remove the SiO_2 underneath the nanocantilevers, while retaining most of the SiO_2 underneath the frame structure between neighboring c-SRRs (Fig. 2e). This design prevented possible collapse of the entire metamaterial surface under an applied voltage. Finally, a ~20-nm-thick Au thin film was evaporated onto the surface of the device through evaporation. Thus, the Au/Si c-SRRs on the top and Au solid SRRs at the bottom of the air cavities were formed (Fig. 2f). The resulting vertical separation between the c-SRRs and SRRs was ~250 nm. Fig. 2g and 2h show the unreleased and released cantilever after BOE etching of the buried oxide for 3.5 min and 5 min, respectively.

B. Numerical Simulation

Optical simulations were carried out using finite-element-method-based software (COMSOL Multiphysics). The geometrical parameters used in the simulations were extracted from the SEM images of the fabricated device. In the simulations, the thick handling Si layer of the SOI substrate was not included in the computed region due to limited computation power. For simplicity, the rounded 90 degree corners and

Authorized licensed use limited to: Iowa State University. Downloaded on June 04,2022 at 12:40:41 UTC from IEEE Xplore. Restrictions apply.

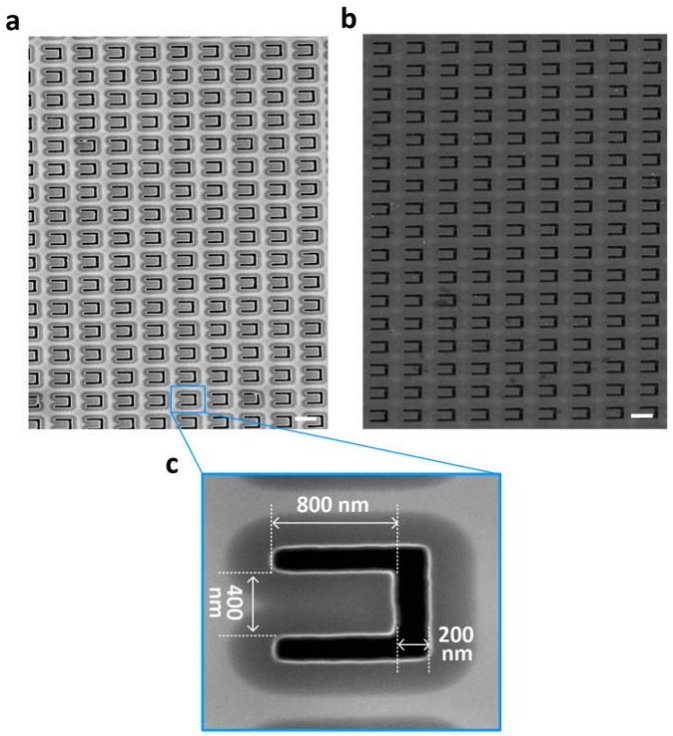

Fig. 3. SEM images of the metamaterial before (a) and after (b) coating with a 20 nm-thick Au layer. The scale bars represent 1 μm. In (a), the cantilevers are released. In (b), the metamaterial is formed. A closed-up of the c-SRR without an Au layer is displayed in (c).

geometrical irregularities of the fabricated c-SRRs occurring in the experiments were not considered.

C. Electro-Optical Characterization

The reflection spectra of metamaterials were measured via the Fourier transform IR (FTIR) microscope system (Hyperion 2000, Bruker) for normal incidence of light. Transverse magnetic (TM) and transverse electric (TE) polarizations were obtained using the built-in polarizers of the FTIR microscope. A D.C. voltage was applied between the gold-coated top surface of the device and the silicon handling layer of the SOI wafer to electrostatically tune the metamaterials during the reflection spectra measurement.

Electro-optical modulation of the metamaterials was conducted by measuring the reflectance change in a 2.1 μm laser beam (Ho:YAG end-pump laser) reflected from the metamaterials, while modulating the metamaterial with a function generator (FG; Agilent 81101A) and a voltage amplifier. The reflected laser beam was detected by an InGaAs photodetector (818-BB-51, Newport) and a lock-in amplifier (SR830, Stanford Research). The whole optical setup for the electro-optical modulation is displayed in the Results and Discussion section.

IV. Results and Discussion

Fig. 3 shows the SEM images of the metamaterial before and after gold coating at the surface of the device. Fig. 4a

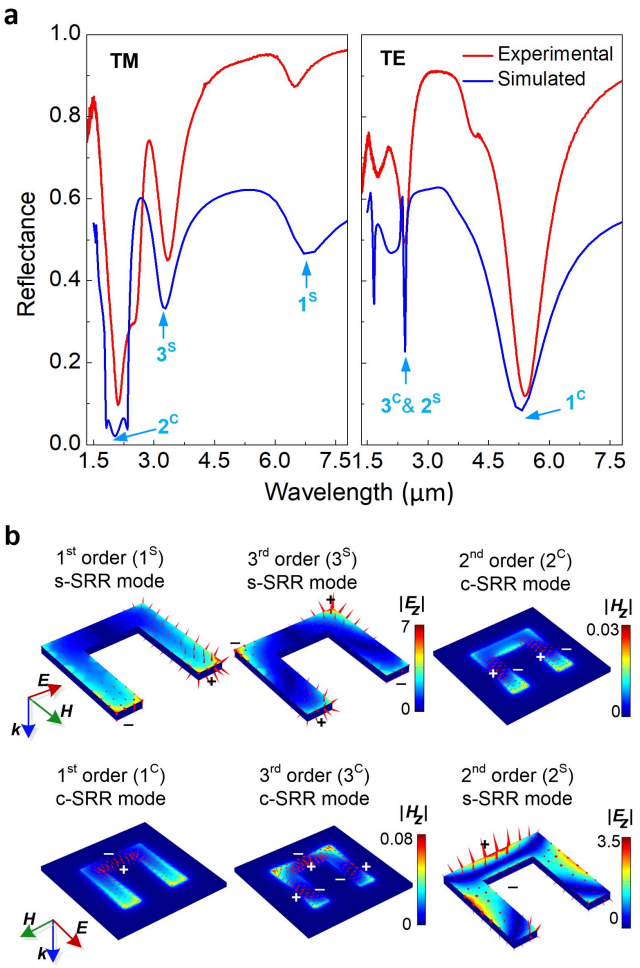

Fig. 4. (a) Measured and simulated reflection spectra of the metamaterial under TM and TE polarizations. Notations 1^S-3^S and 1^C-3^C represent the different orders of the s-SRR and c-SRR modes, respectively. (b) Simulated field distributions of c-SRR and s-SRR modes. The intensity of incident electric field is $E_0 = 1$ V/m. The units of the electric field strength (E_z) and magnetic field strength (H_z) are V/m and A/m, respectively. The arrows in the field distributions denote the electric field, where their directions indicate the vector directions of surface currents.

presents the measured and simulated optical reflection spectra of the metamaterial under TM and TE polarizations when no voltage is applied to the metamaterial. Conspicuous resonance dips are observed at different wavelengths. In general, when the incident field is polarized along the parallel (TM) or perpendicular (TE) directions to their gaps, odd or even eigenmodes will be excited for SRRs [35]. In contrast, even or odd eigenmodes of c-SRRs will be excited by TM- or TE-polarized fields, respectively. Therefore, for TM polarizations (Fig. 4a; left panel), one even c-SRR mode and two odd s-SRR resonance modes appear as reflectance dips. Here we mark these resonance modes with '1^S' at a wavelength of 6.8 μm, '3^S' at 3.3 μm, and '2^C' at 2.1 μm in the spectrum, where the superscripts 'S' and 'C' denote the modes of the s-SRR and c-SRR, respectively. The origins of these resonances are unveiled by the computed field distributions in Fig. 4c, where the orders of eigenmodes can be defined by the number of nodes in the electric- or magnetic-field component normal to the surface of the s-SRR or c-SRR structure [35], [36].

Authorized licensed use limited to: Iowa State University. Downloaded on June 04,2022 at 12:40:41 UTC from IEEE Xplore. Restrictions apply.

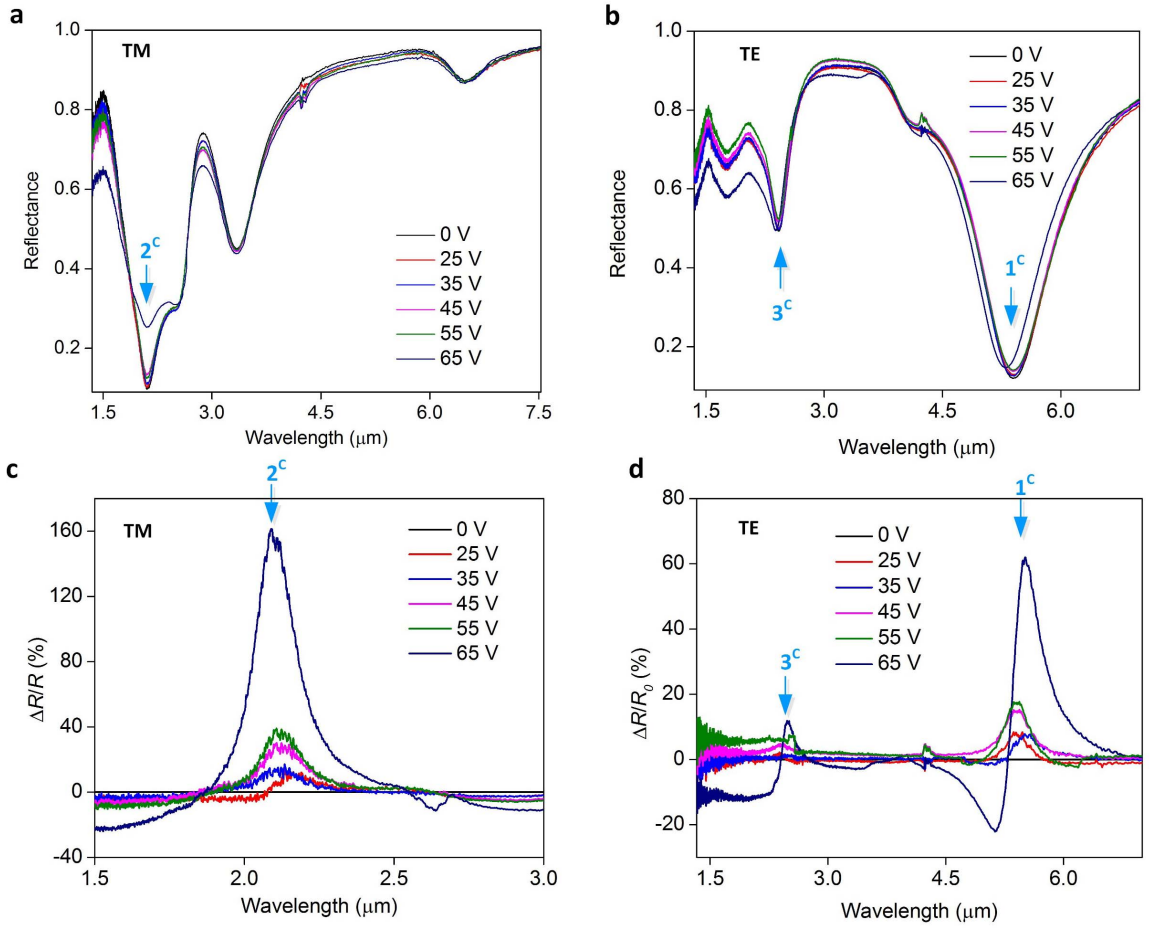

Fig. 5. NEMS-enabled tuning of spectral characteristics of the metamaterial using 0.8 μm-long cantilevers. (a, b) Reflection spectra for different applied voltages under TM (a) and TE (b) polarizations. At 65 V, the cantilevers of the metamaterial are in the pull-in state. (c, d) Spectra of relative reflectance change $\Delta R/R_0$ for different applied voltages under TM (c) and TE (d) polarizations.

For TE polarizations, two odd-order c-SRR resonances (1^C at 5.3 μm and 3^C at 2.5 μm) are excited (Fig. 4a; right panel), as confirmed by the magnetic field distributions in Fig. 4b. However, no distinct resonance dip associated with an even-order s-SRR resonance is observed. Actually, an asymmetric Fano line shape is exhibited near mode 3^C. This originates from the plasmon mode overlap between modes 2^S and 3^C, as confirmed by the electric field distribution of mode 2^S in Fig. 2d, where two amplitude nodes of the electric field are observed. It is worthy to note that no obvious coupling is observed between 1^C or 1^S modes. This is because the s-SRRs are formed with the use of the c-SRRs as shadow masks during deposition of the Au layer, the s-SRRs and c-SRRs are identically shaped and orientated as a solid-inverse structure [37]. It should be noted that the discrepancies between the simulated and experimental results may be caused by the imperfection of the simulation model. The modeling accuracy mainly depends on how accurate the extracted geometric parameters of the c-SRR and s-SRR are. The geometric errors of the model influence the optical resonances of the device, particularly more significant for high-order resonances. The removal of the handling Si layer of the SOI substrate

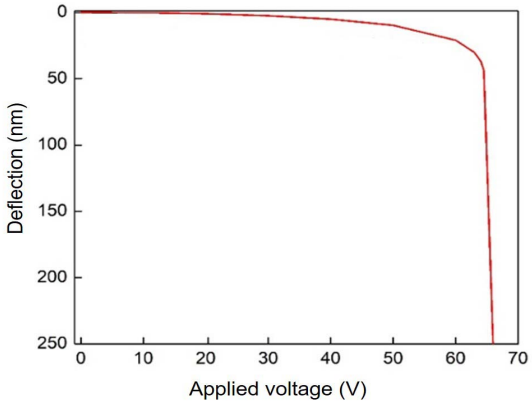

Fig. 6. Simulated mechanical deflection of the cantilever with the length of 0.8 μm under various applied voltages.

from the limited computed region (mentioned in Section III.B) also impacts the reflection intensity. In addition, due to the nanofabrication, the inevitable non-uniformity of the fabricated meta-atoms may be another cause of the discrepancies between the simulated and experimental spectra. Nevertheless, the

Authorized licensed use limited to: Iowa State University. Downloaded on June 04,2022 at 12:40:41 UTC from IEEE Xplore. Restrictions apply.

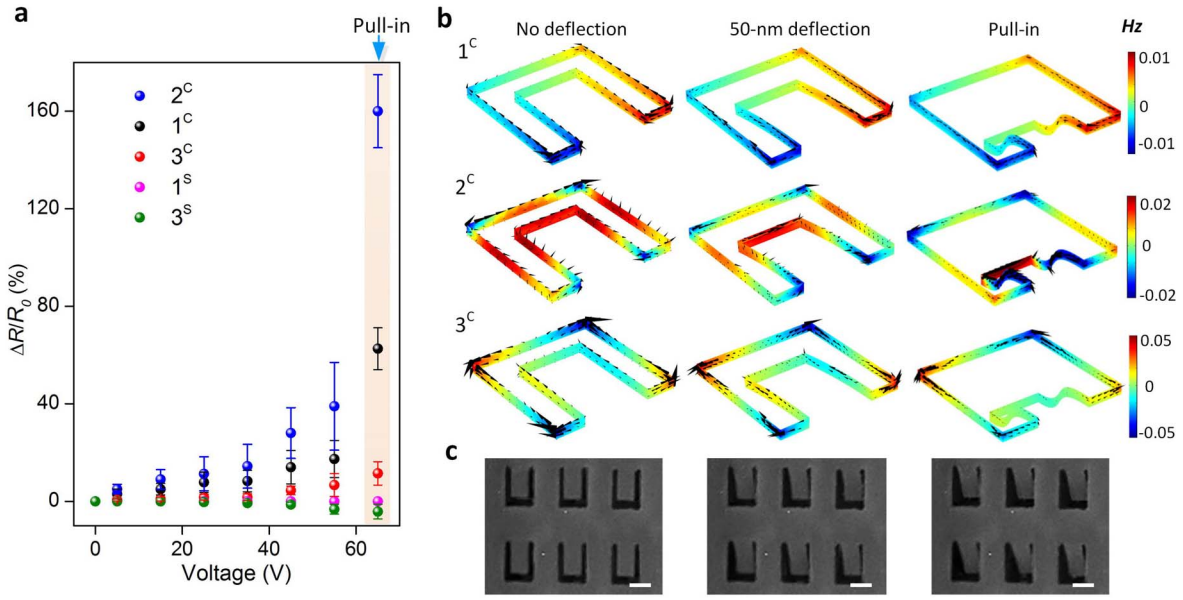

Fig. 7. Effect of applied voltage on resonance modes and field distributions. (a) Summary of the relative changes in reflection intensity for different c-SRR and s-SRR modes as functions of the applied voltage. (b) Magnetic field distributions in the 1^C–3^C modes on the sidewalls of the air nanoaperture under the initial state (left column), with 50 nm deflection (middle column), and the pull-in state (right column) of the nanocantilever. The arrows in the field distributions indicate the vector directions of surface currents. (c) SEM photographs of the metamaterial in the three states shown in (b). The scale bars present 500 nm.

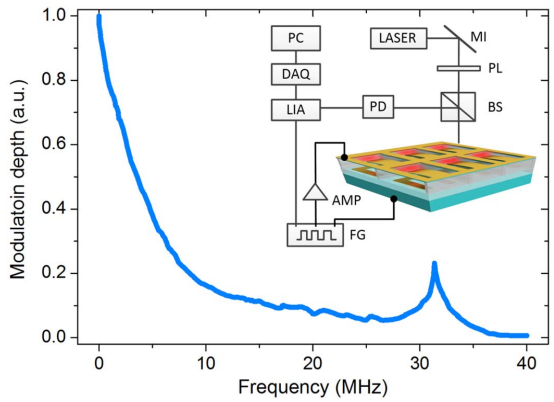

Fig. 8. Normalized modulation depth of the tunable metamaterial as a function of driving frequency. The metamaterial utilizes 0.8 μm-long cantilevers. The inset illustrates the setup. MI – mirror; PL – polarizer; BS – beam splitter; PD – photodetector; LIA – lock-in amplifier; DAQ – data acquisition; FG – function generator; AMP – amplifier; PC – personal computer.

simulations still provide a useful prediction in the wavelengths and line shapes of the resonances that help us to identify the origin of the resonance modes.

We now discuss the influence of applied voltage on the resonance characteristics for the major resonance modes of the metamaterial. As shown in Fig. 5a and b, as the voltage increases from 0 to 55 V, the reflectance dips, assigned to the 1^C, 2^C, and 3^C modes, all exhibit positive changes consistently. The changes of optical signals are caused by the bending of nanocantilevers that change the shapes of c-SRRs. In order to highlight the voltage induced variations, we plot in Fig. 5c and d the relative changes in reflectance at different voltages: $\Delta R/R_o = (R - R_o)/R_o$, where R and R_o represent the reflection intensities at a given voltage and no voltage, respectively. Here one can see that the spectra of $\Delta R/R_o$ show peak-like features. As voltage increases, all the c-SRR modes exhibit a positive change in reflectance. For example, when the applied voltage increases from 0 V to 55 V, the reflectance at the 2^C mode progressively increases from 9.8% to 13.5% (Fig. 5a). This corresponds to a relative reflectance change of $\Delta R/R_o = 38\%$ (Fig. 5c). Accordingly, the values of $\Delta R/R_o$ at the 1^C and 3^C modes are 15% and 5% respectively when applying a voltage of 55 V (Fig. 5d). At higher voltages, the pull-in effect of the nanocantilever occurs due to the strongly nonlinear increase in the electrostatic force, thus causing abrupt deflection and stiction of the nanocantilever to the bottom of the SiO_2 well. The pull-in voltage V_P for a bilayer nanocantilever beam with dimensions of L (length) $\times$ w (width) $\times$ t (thickness) can be estimated using the following equation [38], [39]:

$$V_P = \sqrt{8k_{eff}(d + t_{oxide}/\varepsilon_r)^3/(27\varepsilon_0 wL)} \qquad \text{Eq. (1)}$$

where k_{eff} represents the effective stiffness of the nanocantilever, $d = 250$ nm the distance between the nanocantilever and the bottom of the well, $t_{oxide} = 750$ nm is the thickness of the remaining SiO_2 layer at the bottom of the well, $\varepsilon_r = 3.9$ is the dielectric constant of SiO_2, and ε_o is the permittivity of vacuum. For the given design parameters of $L = 800$ nm, $w = 500$ nm, and $t = 40$ nm, the calculated pull-in voltage was $V_P = 66$ V, which is close to the experimental result of 65 V. Fig. 6 shows the simulated deflection of the nanocantilever under various applied voltages. The result shows the deflection increases slowly below the pull-in voltage, but changes drastically when the voltage approaches the pull-in voltage. In the pull-in state of the nanocantilevers,

Authorized licensed use limited to: Iowa State University. Downloaded on June 04,2022 at 12:40:41 UTC from IEEE Xplore. Restrictions apply.

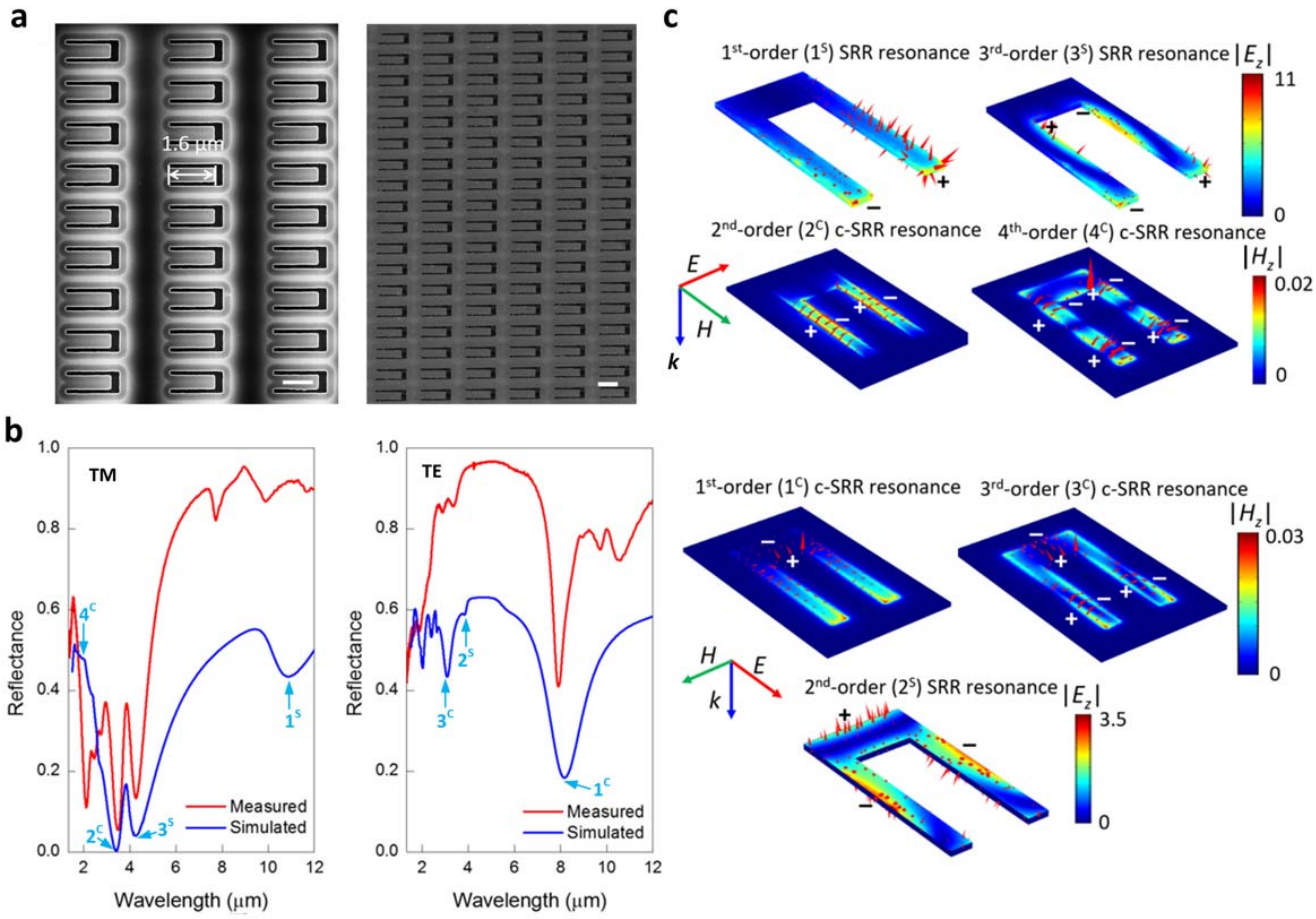

Fig. 9. Tunable metamaterial using 1.6-μm-long cantilevers. (a) SEM photographs of the metamaterial with 1.6-μm-long cantilevers before (left) and after (right) coating of Au layer. The scale bars represent 1 μm. (b) Measured and simulated reflection spectra of the metamaterial for TM (left) and TE (right) polarizations. Notations $1^S - 3^S$ and $1^C - 4^C$ indicate the different orders of the s-SRR and c-SRR modes, respectively. (c) Simulated field distributions of the c-SRR or SRR resonance modes. The intensity of incident electric field is $E_0 = 1$ V/m. The units of the electric field strength (E_z) and magnetic field strength (H_z) are V/m and A/m, respectively. The arrows in the field distributions indicate the electric field, where their directions indicate the phase relation.

the reflectance of the metamaterial at the 2^C mode dramatically increases to 25.5% (Fig. 5a) and thus the corresponding value of $\Delta R/R_o$ reaches 160% (Fig. 5c).

In Fig. 7a, we summarize the reflection intensity modulations for the resonance modes of the metamaterial for different applied voltages. Here one can see that, when applying voltages, the even-order (2^C) c-SRR modes exhibit more significant changes in reflectance than odd-order modes (1^C and 3^C). As the s-SRR structure is unchanged, only minor reflectance changes are observed. For example, the 1^S mode of s-SRR is hardly influenced by the applied voltage and the 3^S mode exhibits only a 3% reduction in $\Delta R/R_o$.

To understand the changes of the c-SRR modes caused by the deflection of the nanocantilever, we computed the field distributions corresponding to the 1^C, 2^C, and 3^C resonance modes under different nanocantilever bending conditions, as shown in Fig. 7b. The incident EM field leads to currents flowing in opposite directions on the concave and convex surfaces of the nanoapertures, thus forming a waveguide mode inside the nanoaperture [40]. Alternatively, the c-SRR resonances can essentially be understood as Fabry–Pérot resonances of guided waves propagating perpendicular to the nanoaperture [36]. The widening gap of the nanoaperture under an applied voltage leads to blue-shift of the resonance wavelength and reduced reflection intensity, owing to weakened near-field interactions around the sidewalls of nanoaperture. The even-order c-SRR modes are more sensitive to the shape change of the nanoaperture compared to the odd-order modes. A plausible explanation for this observation is given below. The field strength is the highest at the amplitude node. For the odd-order modes, the current flow starts at the front sidewall of the nanocantilever and ends at the opposite surface across the gap. The magnetic field intensities at these surfaces are low (close to zero). In contrast, for the even-order modes, the current flow starts and ends at the corners of the nanoaperture, and thus, the front sidewall of the nanocantilever serves as one of the amplitude nodes, where the nanocantilever has strong near-field interactions with its opposite surface. As a result, these even-order modes are more sensitive to changes of the nanoaperture size. As shown in Fig. 7b, a 50 nm deflection at the tip of the nanocantilever causes significant changes in the current and magnetic field density in the 2^C mode at the front sidewall of the nanocantilever, whereas very little change is observed in the 1^C and 3^C modes. In the pull-in state,

Authorized licensed use limited to: Iowa State University. Downloaded on June 04,2022 at 12:40:41 UTC from IEEE Xplore. Restrictions apply.

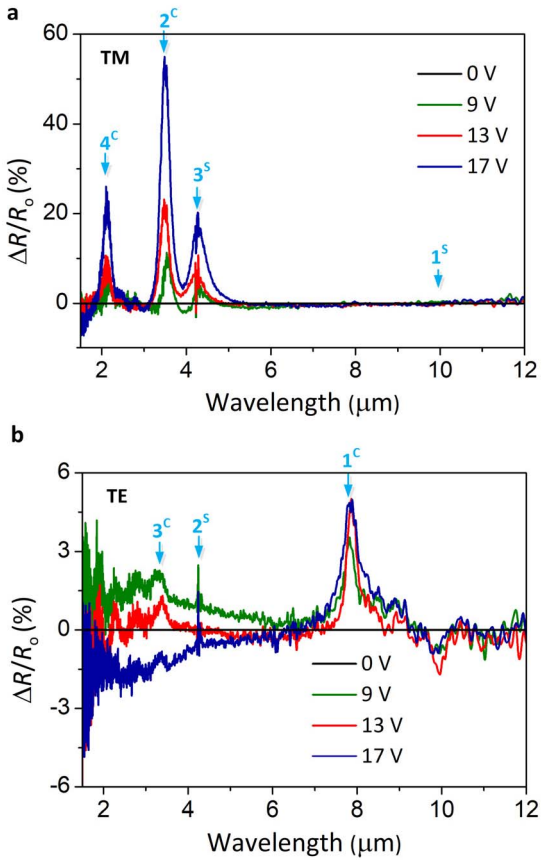

Fig. 10. Spectra of relative reflectance change $\Delta R/R_o$ of the tunable metamaterial using 1.6 μm-long cantilevers for TM (a) and TE (b) polarizations under different applied voltages. The voltages applied here are below the 20.5 V pull-in voltage of the embedded cantilever.

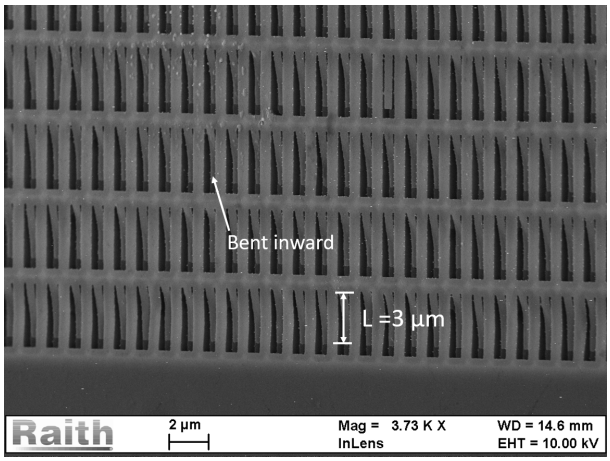

Fig. 11. SEM photo of the metamaterial with 3-μm-long cantilevers.

both 1^C and 3^C c-SRR modes still exist but are insensitive to the deflection of the nanocantilever, as confirmed by the EM simulation.

Following the above discussions of the device tunability, we examine the electro-optical modulation of the IR metamaterial. As illustrated in the inset of Fig. 8, a 2.1 μm-wavelength laser beam in mode 2^C was made normally incident on the metamaterial. A square-wave driving voltage switching between 0 and 55 V was applied to the metamaterial. The incident laser beam was thus modulated by the metamaterial, and the reflected light was detected by a photodetector. No stiction of the nanocantilevers was observed in this experiment because here, the applied highest voltage was lower than the pull-in voltage of 65 V. At 55 V, the obtained deflection is ~20 nm (Fig. 6), which is insufficient to cause stiction of the cantilever to the bottom of the 250 nm-deep air cavity. Fig. 8 shows the frequency dependences of electro-optic modulation for the metamaterial. The spectral responses exhibit an initial roll-off until 10 MHz and the mechanical resonance frequency exhibits at 32.26 MHz, which agrees well with the simulated frequency of 31.35 MHz. Here, the normalized modulation depth at the mechanical resonance frequency is 24%, in which the reflectance obtained at the mechanical resonance frequency of 31.35 MHz is normalized to the one obtained at 55 V DC input. The absolute modulation depth can be calculated as $(1+0.24)\times(\Delta R/R_o) = 1.24\times 38\% = 47\%$, where $\Delta R/R_o = 38\%$ is the relative reflectance change at the 2^C resonance mode of the metamaterial (Fig. 5c). This result indicates that the metamaterial can be driven to its fundamental resonance frequency. In essence, the electro-optic effect of the tunable metamaterial originates from the electrostatically induced mechanical deformation of the c-SRRs, affecting the effective refractive index of each optical resonant element and thus the resonance characteristics of the metamaterial. In contrast, conventional electro-optic materials such as electrified crystals often have millimetre-scale dimensions and use birefringence-induced polarization effects with the aid of polarizers [41]. Meanwhile, liquid-crystal-based electro-optic modulators [15], [42], [43] provide slow responses due to the slow reorientation process of the liquid-crystal molecules, which limits their modulation frequency. In contrast, via constructing c-SRRs with free-standing Au–Si nanocantilevers at the subwavelength scale, we can tune the optical resonances of the formed metamaterials to modulate the incident waves by applying an electrical potential. The complementary structural feature of the optical resonators also simplifies the nanomanufacturing processes and the driving method for electro-optic modulations in the near-to-mid-IR spectral regime. Further, the resulting small dimensions of the meta-atoms lead to high mechanical resonance frequencies of the order of several tens of MHz, i.e. one to three order of magnitude higher than almost all existing reconfigurable metamaterials [21]–[29]. An optomechanical dielectric metamaterial [44] was recently reported to exhibit a higher modulation frequency; however, owing to the weak optical force, the metamaterial provided a limited maximum modulation depth of 0.2% (normalized value) [44]. In comparison, our metamaterial, when operating at its mechanical resonance frequency, offers the normalized modulation depth of 24%, about two orders of magnitude higher than the metamaterial using the optical force [44]. This is because the electrostatic actuation method used in our device allows larger deflections of the cantilever than the optomechanical actuation method.

Although the nanocantilever stiction at pull-in is irreversible due to van der Waals interactions, the stiction could be avoided

Authorized licensed use limited to: Iowa State University. Downloaded on June 04,2022 at 12:40:41 UTC from IEEE Xplore. Restrictions apply.

by some methods such as using closed-loop control and proper surface treatment to extend the range of travel for the nanocantilever [39]. In addition, to achieve larger tunability of the EM resonances with lower driving voltages, design improvements can be made. Possible optimization includes introducing appropriate structural symmetry breaking between the c-SRR and s-SRR structures to generate stronger coupled resonances in their fundamental modes [37], [45]–[47], thus improving resonance sensitivity of the cantilever deflection. The symmetry breaking could be achieved via formation of overlapping shadow areas between the c-SRR and SRR. Moreover, it is flexible to adjust optical resonance wavelengths of the metamaterial by adjusting the geometries and dimensions of nanoapertures and cantilevers. For example, Fig. 9a shows the metamaterial with 1.6 μm-long cantilevers embedded in the c-SRRs. The resonance wavelength of the 2^{C} c-SRR mode for this metamaterial redshifts to a longer wavelength at 3.41 μm (Fig. 9b; left panel), compared to the mode wavelength of 2.1 μm for the above-mentioned metamaterial using 0.8 μm-long cantilevers. Similarly, to identify the origins of the resonance dips displayed in Fig. 9b, we computed the field distributions of the c-SRR or SRR resonance modes in Fig. 9c. Further, Fig. 10 shows the TE and TM spectra for the relative reflectance change $\Delta R/R_{\mathrm{o}}$ of the metamaterial with 1.6 μm-long cantilevers under different applied voltages before the pull-in effect occurs at 20.5 V. As expected, with increasing applied voltages from 0 to 17 V, the 1^{C} and 3^{C} c-SRR modes for TE polarizations and the 1^{S} s-SRR mode for TM polarizations exhibit relatively low sensitivities to the applied voltages. The maximum value of $\Delta R/R_{\mathrm{o}}$ is found to be 58% at the 2^{C} mode at 17 V (Fig. 10). The electro-optic modulation experiment indicates that due to the longer cantilevers embedded in the c-SRR structures, this metamaterial exhibits a lower mechanical modulation frequency of 5.32 MHz, compared to the above-described one using 0.8 μm-long cantilevers (i.e., 32.26 MHz).

Lastly, it should be noted that in this design, the length of the Au-coated cantilevers should be no more than 3 μm to avoid significant initial bending. Fig. 11 shows that when the metamaterial has 3 μm-long cantilevers, even in the absence of voltage application the thin cantilevers (20-nm-thick silicon and 20 nm-thick gold) are already bent into the wells, perhaps owing to the initial stress of the cantilevers.

V. Conclusions

In summary, we have demonstrated the NEMS-enabled tunable metamaterials operating in the near-to-mid-IR range by electromechanically tuning the nanocantilevers embedded in the c-SRR units. As the nanocantilevers bend downward towards the substrate, the U-shaped air gaps in the c-SRRs are geometrically changed, thus altering the surface-current flows on the sidewalls of the nanoapertures and varying the resonance intensity. The deflection of the nanocantilevers leads to significantly larger changes in the even c-SRR modes, while this change is less impactful in the odd c-SRR and SRR modes. With the compact and easy-to-implement meta-atom design, the present tunable metamaterial can provide fast electro-optic modulation at frequencies of several tens of MHz. In addition, this technology will find many applications in optical modulators, infrared sensors [48], and transformation optics [49]. Our tunable metamaterial design may also shed a light on a reconfigurable metamaterial where each resonant element may be individually controlled via integration of CMOS based integrated circuits within the top silicon device layer of SOI substrate.

Acknowledgment

The authors would like to thank the Microelectronics Research Center at the Iowa State University, Ames, Iowa, and the Minnesota Nano Center at the University of Minnesota, Twin City, MN, for semiconductor fabrication facilities, and Dr. Siming Yang, Prof. Jiming Song, Prof. Robert J. Weber, and Prof. Zhe Fei for their helpful discussions.

References

[1] N. Fang, H. Lee, C. Sun, and X. Zhang, "Sub–diffraction-limited optical imaging with a silver superlens," *Science*, vol. 308, no. 5721, p. 534, Apr. 2005.

[2] I. Smolyaninov, II, Y.-J. Hung, and C. C. Davis, "Magnifying superlens in the visible frequency range," *Science*, vol. 315, no. 5819, p. 1699, Mar. 2007.

[3] D. Schurig *et al.*, "Metamaterial electromagnetic cloak at microwave frequencies," *Science*, vol. 314, no. 5801, pp. 977–980, Oct. 2006.

[4] S. Yang, P. Liu, M. Yang, Q. Wang, J. Song, and L. Dong, "From flexible and stretchable meta-atom to metamaterial: A wearable microwave meta-skin with tunable frequency selective and cloaking effects," *Sci. Rep.*, vol. 6, Feb. 2016, Art. no. 21921.

[5] N. I. Landy, S. Sajuyigbe, J. J. Mock, D. R. Smith, and W. J. Padilla, "Perfect metamaterial absorber," *Phys. Rev. Lett.*, vol. 100, no. 20, p. 207402, May 2008.

[6] N. Liu, M. Mesch, T. Weiss, M. Hentschel, and H. Giessen, "Infrared perfect absorber and its application as plasmonic sensor," *Nano Lett.*, vol. 10, no. 7, pp. 2342–2348, 2010.

[7] A. V. Kabashin *et al.*, "Plasmonic nanorod metamaterials for biosensing," *Nature Mater.*, vol. 8, no. 11, pp. 867–871, Nov. 2009.

[8] I. M. Pryce, Y. A. Kelaita, K. Aydin, and H. A. Atwater, "Compliant metamaterials for resonantly enhanced infrared absorption spectroscopy and refractive index sensing," *ACS Nano*, vol. 5, no. 10, pp. 8167–8174, Oct. 2011.

[9] X. Xu *et al.*, "Flexible visible–infrared metamaterials and their applications in highly sensitive chemical and biological sensing," *Nano Lett.*, vol. 11, no. 8, pp. 3232–3238, Aug. 2011.

[10] N. I. Zheludev and Y. S. Kivshar, "From metamaterials to metadevices," *Nature Mater.*, vol. 11, pp. 917–924, Nov. 2012.

[11] M. Seo *et al.*, "Active terahertz nanoantennas based on VO_2 phase transition," *Nano Lett.*, vol. 10, no. 6, pp. 2064–2068, Jun. 2010.

[12] T. Driscoll *et al.*, "Dynamic tuning of an infrared hybrid-metamaterial resonance using vanadium dioxide," *Appl. Phys. Lett.*, vol. 93, no. 2, p. 024101, Jul. 2008.

[13] Q. Wang *et al.*, "Tunable optical nanoantennas incorporating bowtie nanoantenna arrays with stimuli-responsive polymer," *Sci. Rep.*, vol. 5, p. 18567, Dec. 2015.

[14] A. Minovich, D. N. Neshev, D. A. Powell, I. V. Shadrivov, and Y. S. Kivshar, "Tunable fishnet metamaterials infiltrated by liquid crystals," *Appl. Phys. Lett.*, vol. 96, no. 19, p. 193103, May 2010.

[15] D. Shrekenhamer, W. C. Chen, and W. J. Padilla, "Liquid crystal tunable metamaterial absorber," *Phys. Rev. Lett.*, vol. 110, no. 17, p. 177403, Apr. 2013.

[16] B. Grzeskiewicz, E. Wolarz, A. Sierakowski, J. Marczewski, and N. Palka, "Liquid crystal-tunable metamaterial absorber for THz frequency range," in *Proc. 7th Int. Congr. Adv. Electromagn. Mater. Microw. Opt. (Metamater.)*, Sep. 2013, pp. 178–180.

[17] S. M. Xiao, U. K. Chettiar, A. V. Kildishev, V. Drachev, I. C. Khoo, and V. M. Shalaev, "Tunable magnetic response of metamaterials," *Appl. Phys. Lett.*, vol. 95, no. 3, p. 033115, Jul. 2009.

Authorized licensed use limited to: Iowa State University. Downloaded on June 04,2022 at 12:40:41 UTC from IEEE Xplore. Restrictions apply.

[18] H.-T. Chen, W. J. Padilla, J. M. O. Zide, A. C. Gossard, A. J. Taylor, and R. D. Averitt, "Active terahertz metamaterial devices," *Nature*, vol. 444, pp. 597–600, Oct. 2006.
[19] N. H. Shen *et al.*, "Optically implemented broadband blueshift switch in the terahertz regime," *Phys. Rev. Lett.*, vol. 106, no. 3, p. 037403, Jan. 2011.
[20] Y. Urzhumov *et al.*, "Electronically reconfigurable metal-on-silicon metamaterial," *Phys. Rev. B, Condens. Matter*, vol. 86, no. 7, p. 075112, Aug. 2012.
[21] N. I. Zheludev and E. Plum, "Reconfigurable nanomechanical photonic metamaterials," *Nature Nanotechnol.*, vol. 11, no. 1, pp. 16–22, Jan. 2016.
[22] H. Tao, A. C. Strikwerda, K. Fan, W. J. Padilla, X. Zhang, and R. D. Averitt, "Reconfigurable terahertz metamaterials," *Phys. Rev. Lett.*, vol. 103, no. 14, p. 147401, Oct. 2009.
[23] J. Y. Ou, E. Plum, L. Jiang, and N. I. Zheludev, "Reconfigurable photonic metamaterials," *Nano Lett.*, vol. 11, no. 5, pp. 2142–2144, May 2011.
[24] C. P. Ho, P. Pitchappa, Y. S. Lin, C.-Y. Huang, P. Kropelnicki, and C. Lee, "Electrothermally actuated microelectromechanical systems based omega-ring terahertz metamaterial with polarization dependent characteristics," *Appl. Phys. Lett.*, vol. 104, no. 16, p. 161104, Apr. 2014.
[25] F. Ma, Y.-S. Lin, X. Zhang, and C. Lee, "Tunable multiband terahertz metamaterials using a reconfigurable electric split-ring resonator array," *Light, Sci. Appl.*, vol. 3, p. e171, May 2014.
[26] W. M. Zhu *et al.*, "Switchable magnetic metamaterials using micromachining processes," *Adv. Mater.*, vol. 23, no. 15, pp. 1792–1796, Apr. 2011.
[27] W. M. Zhu *et al.*, "Microelectromechanical maltese-cross metamaterial with tunable terahertz anisotropy," *Nature Commun.*, vol. 3, p. 1274, Dec. 2012.
[28] Y. H. Fu *et al.*, "A micromachined reconfigurable metamaterial via reconfiguration of asymmetric split-ring resonators," *Adv. Funct. Mater.*, vol. 21, no. 18, pp. 3589–3594, Sep. 2011.
[29] X. Zhao *et al.*, "Voltage-tunable dual-layer terahertz metamaterials," *Microsyst. Nanoeng.*, vol. 2, p. 16025, Jul. 2016.
[30] P. Pitchappa, C. P. Ho, P. Kropelnicki, N. Singh, D. L. Kwong, and C. Lee, "Micro-electro-mechanically switchable near infrared complementary metamaterial absorber," *Appl. Phys. Lett.*, vol. 104, no. 20, p. 201114, May 2014.
[31] X. L. Liu and W. J. Padilla, "Dynamic manipulation of infrared radiation with MEMS metamaterials," *Adv. Opt. Mater.*, vol. 1, no. 8, pp. 559–562, Aug. 2013.
[32] J.-Y. Ou, E. Plum, J. Zhang, and N. I. Zheludev, "An electromechanically reconfigurable plasmonic metamaterial operating in the near-infrared," *Nature Nanotechnol.*, vol. 8, no. 4, pp. 252–255, Mar. 2013.
[33] J. Y. Ou, E. Plum, J. Zhang, and N. I. Zheludev, "Giant nonlinearity of an optically reconfigurable plasmonic metamaterial," *Adv. Mater.*, vol. 28, no. 4, pp. 729–733, Jan. 2016.
[34] J. Valente, J. Y. Ou, E. Plum, I. J. Youngs, and N. I. Zheludev, "A magneto-electro-optical effect in a plasmonic nanowire material," *Nature Commun.*, vol. 6, p. 7021, Apr. 2015.
[35] C. Rockstuhl, F. Lederer, C. Etrich, T. Zentgraf, J. Kuhl, and H. Giessen, "On the reinterpretation of resonances in split-ring-resonators at normal incidence," *Opt. Exp.*, vol. 14, no. 19, pp. 8827–8836, Sep. 2006.
[36] C. Rockstuhl, T. Zentgraf, T. P. Meyrath, H. Giessen, and F. Lederer, "Resonances in complementary metamaterials and nanoapertures," *Opt. Exp.*, vol. 16, no. 3, pp. 2080–2090, Feb. 2008.
[37] M. Hentschel, T. Weiss, S. Bagheri, and H. Giessen, "Babinet to the half: Coupling of solid and inverse plasmonic structures," *Nano Lett.*, vol. 13, no. 9, pp. 4428–4433, Sep. 2013.
[38] S. Chowdhury, M. Ahmadi, and W. C. Miller, "A closed-form model for the pull-in voltage of electrostatically actuated cantilever beams," *J. Micromech. Microeng.*, vol. 15, no. 4, pp. 756–763, Apr. 2005.
[39] W.-M. Zhang, H. Yan, Z.-K. Peng, and G. Meng, "Electrostatic pull-in instability in MEMS/NEMs: A review," *Sens. Actuators A, Phys.*, vol. 214, pp. 187–218, Aug. 2014.
[40] J. A. Porto, F. J. García-Vidal, and J. B. Pendry, "Transmission resonances on metallic gratings with very narrow slits," *Phys. Rev. Lett.*, vol. 83, no. 14, pp. 2845–2848, Oct. 1999.
[41] K. Noguchi, O. Mitomi, and H. Miyazawa, "Millimeter-wave Ti: $LiNbO_3$ optical modulators," *J. Lightw. Technol.*, vol. 16, no. 4, pp. 615–619, Apr. 1998.
[42] L. Vicari, *Optical applications of liquid crystals*. Philadelphia, PA, USA: Inst. Phys. Pub., 2003.
[43] Q. Wang, W. Han, P. Liu, and L. Dong, "Electrically tunable quasi-3-D mushroom plasmonic crystal," *J. Lightw. Technol.*, vol. 34, no. 9, pp. 2175–2181, May 2016.
[44] A. Karvounis, J.-Y. Ou, W. Wu, K. F. MacDonald, and N. I. Zheludev, "Nano-optomechanical nonlinear dielectric metamaterials," *Appl. Phys. Lett.*, vol. 107, no. 19, p. 191110, Nov. 2015.
[45] H. T. Chen *et al.*, "Complementary planar terahertz metamaterials," *Opt. Exp.*, vol. 15, no. 3, pp. 1084–1095, Feb. 2007.
[46] S. Wu *et al.*, "Asymmetric transmission and optical rotation of a quasi-3D asymmetric metallic structure," *Opt. Lett.*, vol. 39, no. 22, pp. 6426–6429, Nov. 2014.
[47] K. Aydin *et al.*, "Split-ring-resonator-coupled enhanced transmission through a single subwavelength aperture," *Phys. Rev. Lett.*, vol. 102, no. 1, p. 013904, Jan. 2009.
[48] D. Liang, Y. Rui-Feng, and L. Li-Tian, "Characterization of uncooled poly SiGe microbolometer for infrared detection," *Chin. Phys. Lett.*, vol. 20, no. 5, pp. 770–773, May 2003.
[49] Y. Wang, J. Song, L. Dong, and M. Lu, "Optical bound states in slotted high-contrast gratings," *J. Opt. Soc. Amer. B*, vol. 33, no. 12, pp. 2472–2479, Dec. 2016.

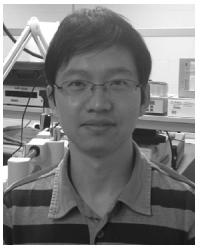

Qiugu Wang received the B.S. and M.S. degrees in physics from Nanjing University, China, in 2009 and 2012, respectively. He is currently pursuing the doctoral degree with the Department of Electrical and Computer Engineering, Iowa State University. His research interests include optical MEMS, plasmonics, metamaterials, and sensors.

Depeng Mao received the B.S. degree in thermal energy and power engineering from the Huazhong University of Science and Technology, China, in 2003; the M.S. degree in optics from Shenzhen University, China, in 2008; and the Ph.D. degree in electrical engineering from Iowa State University, in 2013. He is currently an Engineer with Microsoft, Redmond, WA, USA.

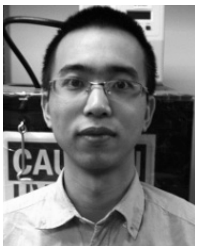

Peng Liu received the B.S. degree in physics and the M.S. degree in electrical engineering from the Dalian University of Technology, China, in 2007 and 2010, respectively, and the Ph.D. degree in electrical engineering from Iowa State University, in 2015. He is currently an Engineer with Epic Systems Corporation, Verona, WI, USA.

Thomas Koschny received the M.S. and Ph.D. degrees in physics from Universität Leipzig, Leipzig, Germany, in 1997 and 2001, respectively. From 2000 to 2002, he was a Post-Doctoral Researcher of quantum Hall effect at Physikalisch-Technische Bundesanstalt, Braunschweig, Germany. Since 2003, he has been involved in the electromagnetic wave propagation in left-handed metamaterials with the Institute of Electronic Structure and Laser, Foundation for Research and Technology Hellas, Crete, Greece. Since 2004, he has been a Researcher with the Ames Laboratory and the Department of Physics and Astronomy, Iowa State University, Ames, IA, USA. His current research interests include the theory of left-handed metamaterials and photonic crystals.

Authorized licensed use limited to: Iowa State University. Downloaded on June 04,2022 at 12:40:41 UTC from IEEE Xplore. Restrictions apply.

Costas M. Soukoulis received the B.Sc. degree from the University of Athens, in 1974, and the Ph.D. degree in physics from the University of Chicago, in 1978. From 1978 to 1981, he was in the Physics Department, University of Virginia. He spent three years (1981–1984) at Exxon Research and Engineering Company, and since 1984, has been with Iowa State University (ISU) and the Ames Laboratory. He is a Senior Scientist with the Ames Laboratory and a Distinguished Professor of physics with ISU. His research interests are to develop theoretical understanding of the properties of disordered systems, with emphasis on electron and photon localization, photonic crystals, random lasers, and metamaterials. The theoretical models developed are often quite sophisticated to accurately reflect the complexity of real materials. He is a fellow of the APS, OSA, and AAAS. He has served on several boards and committees for organizations, including the NSF, the DOE, and the European Union, and he is a Member of the Editorial Board of PRL. He has been a member or a chairman of various scientific committees responsible for various international conferences. He has been an Associate Member of IESL-FORTH at Heraklion, Crete, since 1983. He received the Senior Humboldt Research Award; he shared the Descartes Award for research on metamaterials and the APS 2013 J. C. McGroddy Prize for the discovery of metamaterials; he received the Honorary Doctorate from Vrije University in Brussels; and received the first Frances M. Craig Endowed Chair in physics at ISU.

Liang Dong received the Ph.D. degree in electronic science and technology from the Institute of Microelectronics, Tsinghua University, Beijing, China, in 2004. From 2004 to 2007, he was a Post-Doctoral Research Associate in the Department of Electrical and Computer Engineering, University of Wisconsin–Madison. He is currently an Associate Professor with the Department of Electrical and Computer Engineering, a Courtesy Associate Professor with the Department of Chemical and Biological Engineering, a Faculty Scholar with the Plant Sciences Institute, and an Associate Director of the Microelectronics Research Center with Iowa State University. He is also an Associate of the U.S. DOE's Ames Laboratory. His current research interests include MEMS, microfluidics, sensors, optics, and micro/nanomanufacturing and their applications in sustainable agriculture and environments, plant sciences, biomedicine, and Internet of Things. He serves as an Editorial Board Member for scientific reports. He previously received the National Science Foundation CAREER Award, the Early Career Engineering Faculty Research Award, the Harpole-Pentair Developing Faculty Award, the Warren B. Boast Undergraduate Teaching Award, and the PSI Faculty Scholar Award, all at Iowa State University. He also received the Top 100 National Outstanding Doctoral Dissertation Award in China and the Academic Rising Star Award from Tsinghua University.

Authorized licensed use limited to: Iowa State University. Downloaded on June 04,2022 at 12:40:41 UTC from IEEE Xplore. Restrictions apply.